Intelligent Automation And Soft Computing, 2019

Vol. 25, no. 4, 865–873
https://doi.org/10.31209/2019.100000090

Finite Element Analysis of a Newly Designed Straight Three-Layered Seale Wire Strand

Chun-Lei Yu[1], Bin-Jie Dong[2]

[1]School of Mechanical and Electrical Engineering, Zaozhuang University, Zaozhuang, Shandong, 277106, PR China
[2]Shijiazhuang King Transportation Equipment CO., LTD, Shijiazhuang, Hebei, 050000, PR China

ABSTRACT

A new geometry design method of three-layered Seale wire strand is proposed. The included angle between adjacent helical wires in the same layer, which is assumed as zero in the conventional design method, can be predefined arbitrarily by using the new method. The key process of deriving the diameter ratio of each layer wires was formulated into a one-dimensional problem and golden section method was applied to solve the problem efficiently. Finite element analysis of the newly developed three-layered Seale strand was also implemented by using a concise finite element model (FEM) which takes full advantage of the helical symmetry and cyclic symmetry of the three-layered Seale strand analysed in this paper. Three-dimensional solid brick elements were used for structural discretization. Nonlinear factors such as inter-wire contact and material plasticity were also taken into account. Numerical results show that the circumferential angle of helical wires is very small for the three-layered Seale strand subjected to axial tensile loads. For the 19-wire Seale strand loaded in the linear region, when included angle is predefined beyond 0.0042°, it can be ensured that the helical wires in the same layer will not touch each other.

KEY WORDS: Seale wire strand, geometry design method, tensile behavior, inter-wire contact, finite element analysis

1 INTRODUCTION

Seale wire strands are a class of important line contact strand and widely employed as the basic components of stranded wire ropes. The major advantage of the structural elements is their capacity to support large axial loads and excellent wear resistance with comparatively small bending stiffness. They have played a vital and useful role in various engineering applications such as cableway, lift and inclined shaft etc.

In general, Seale wire strands are groups of wires laid helically in successive layers over a straight metal or fiber center wire in a regular geometric pattern. They are usually manufactured through one twisting process and every layer wires have the same helical direction and pitch length. Nowadays, the geometry design of the Seale wire strands is implemented mainly depending on strand mechanical properties and the key process is to derive the wire diameter ratio of each layer wires. Gradual approaching method is commonly applied to calculate the wire diameter ratio in engineering applications (Pan and Qiu, 2008). In the implementation of this method, an initial ratio should be calculated based on the wire geometrical parameters of the cross-section of the non-twisting strand firstly. Secondly, considering the actual strand cross-section shape, a new diameter ratio is updated depended on the initial diameter ratio. In this process, the cross-sections of helical wires are assumed as ellipse and those in the same layer are just touching each other. Thirdly, the second process is implemented repeatedly until the computing accuracy meets the engineering requirement. The main limit of this method is that it requires the cross-section shapes of helical wires in the same layer are tangent with each other. Moreover, the calculation precise can not be effectively guaranteed and more times and calculation resources should be invested.

With the development of computer-aided design, progress has been made in strand structure design and

CONTACT Chun-Lei Yu yclfinder@163.com

geometric model establishment of wire rope and strand (2007, 2016). Computing precise and efficiency have been improved greatly and the actual geometric configuration can be easily built by using the three-dimensional modeling software. Erdönmez and Imrak (2011) proposed a modeling technique for the nested helical structure. Frenet-Serret frame located along the central lines of every strand kernel was applied to calculate the derivations of helical parametric equations. Stanova et al. (2011, 2011, 2015) presented the mathematical geometric models of a single-lay wire strand, double-lay wire rope and spiral one or two-layered oval wire strand by establishing the mathematical equations of wire geometric parameters. Three-dimensional modeling software, such as Pro/Engineer Wildfire V 5.0 and CATIA V5, were used to generate their geometric configurations. Wang et al. (2015) developed mathematical geometric models for generating single or multi-layer strands and multi-strands wire rope whose centerlines can be in arbitrary spatial pattern. Mathematical representations on centerlines of wires and strands within ropes and method used for calculating their radii were also presented. Procedures of generating wire rope/strand geometric models were conducted on the CATIA software. Chen et al. (2015) developed a new parametric geometric model of the spiral triangular strand. This model was implemented by means of parameter equations and Pro/Engineer software and detailedly considered the effects of lay angle on the wire cross-section. By using the curve function of UG software, Sun et al. (2016) built the geometric model of Seale wire strand rope. In this model, the geometric relationships between lay angles of the second layer wires and the third layer wires, and that between the radii of these two layers for the Seale wire strand were established in detail. Zhao et al. (2017) developed a mathematical model of a wire strand in the bending state. The transformation matrix of each local coordinate system established along the centerlines of wires or strands was derived.

Except for geometric structure design, Mechanical behavior prediction also plays an important role in the strand design. The methods used to predict the mechanical behavior of wire rope strands can be usually grouped into three main categories, i.e. experimental test, analytical method and finite element method (2000, 2014, 2017). Compared with the first two ones, finite element method is capable of greatly reducing the investment in human and material resources, and detailedly taking into account the actual wire geometry and nonlinear factors which are difficult to address analytically. In particular, with the development of computer software and hardware, finite element method has been widely used in engineering applications and a large number of numerical models have been developed to date. Jiang et al. (1999) developed several concise finite element models (FEMs) of a 7-wire straight strand by using accurate helical symmetry and cyclic symmetry conditions. The mechanical behaviors of strand under axial tensile load and pure bending moment have been efficiently predicted. Moreover, the statically indeterminate contacts (2008) and strand termination effects (1999) have also been studied. Then, Jiang et al. (2000) extended their analysis to a three-layered straight wire strand under axial loads. Another concise FEM which detailedly accounts for the helical symmetry was established. Páczelt et al. (2011) developed a p-version finite element software for a simple straight two layered wire strand. Inter-wire motions, contact and dry friction between wires were considered in this FEM. Moreover, a special nonlinear contact theory, which considers the Poisson effect and wear, has also been presented. Judge et al. (2012) presented full three-dimensional elasto-plastic FEMs of multilayered wire strand cables subjected to axial loads. Analysis was implemented by using LS-DYNA and the mechanical behavior of the multilayered strand cables was predicted effectively. Zhou and Tian (2013) investigated a new FEM for the simple 7-wire straight strand under axial and bending loads. Mathematical model was created by sectional path-nodes sweeping and dynamic node-beam mapping. Fontanari et al. (2015) developed FEMs of Warrington-Seale strands and a Warrington-Seale rope with a polymeric fiber core. Elasto-plastic responses of the strands and rope noted above under axial loads were studied. Finite element analysis results showed good agreement with those predicted by experimental test. Yu et al. (2016) developed a simplified FEM of structural cables under bending moment. In this model, beam elements were used to simulate spiral wires and replace wire sections, and spring elements were employed to capture contact extrusion and friction occurred between adjacent wires. Judge et al. (2017) proposed complex three-dimensional nonlinear FEMs subjected to high velocity fragment impact. By using the model, the cable penetration resistance and resultant damage were predicted.

In this paper, a new geometry design method and geometric model of three-layered 19-wire Seale strand has been established to improve the accuracy and efficiency of Seale strand geometric design. The key process of determining the diameter ratio of each layer wires in the conventional method has been formulated into a one-dimensional problem and efficient golden section method has been employed to solve it instead of gradual approaching method. The included angle between adjacent helical wires in the same layer has also been realized to arbitrarily predefine its value. Moreover, a concise FEM has also been developed to study the tensile behavior of the three-layered 19-wire Seale strand. Accurate boundary conditions have been developed on the basis of the strand helical symmetry and cyclic symmetry. By using the model, the tensile behavior of the 19-wire Seale strand and the effects of

nonlinear factors and strand geometry parameters have been predicted effectively.

2 GEOMETRY DESIGN METHOD AND GEOMETRIC MODEL

The configuration and cross-section of a three-layered Seale wire strand analyzed in this paper is shown in Fig.1. The strand consists of a straight circular center wire with radius R_1, surrounded by m second layer wires with radius R_2, and a further m third layer wires with radius R_3. r_2 and r_3 are helix radii for the 2nd layer wires and the 3rd layer wires respectively. β_2 and β_3 denote the included angles between the adjacent helical wires in the same layer for the two helical wire layers. The basic loading case in the engineering applications, i.e. the strand is subjected with an axial load *F* and an axial moment *M*, is also shown in Fig. 1.

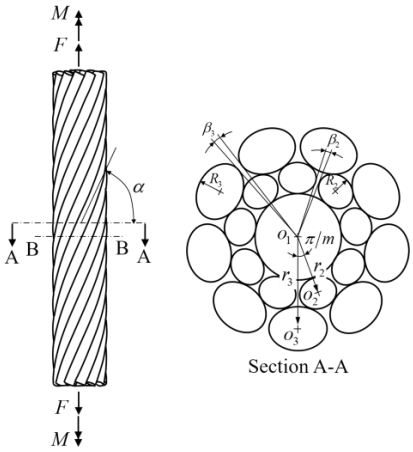

Figure 1. Geometry of three-layered Seale strand

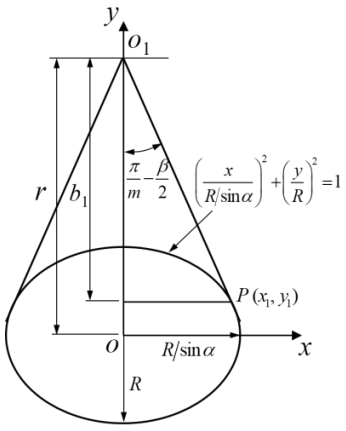

Figure 2. Elliptical cross-section of a helical wire

In this paper, a new geometry design method of the three-layered Seale wire strand is developed. Compared with the conventional strand design method (Pan and Qiu, 2008), the newly presented method allows to predefine the included angles for each layer wires, rather than assumed that they are all zero which means that the helical wires in the same layer are just touching each other. Moreover, the problem of deriving the diameter ratio of each layer wires is formulated into a one-dimensional problem. Golden section method is applied to solve this problem. This greatly raises the computational efficiency and calculation precision, comparing to the gradual approaching method used for deriving the diameter ratio in the conventional design process. The newly developed model is implemented as follows:

(a) calculate helix radius for an arbitrary wire

Fig. 2 shows a helical wire cross-section in a plane perpendicular to the strand symmetric axis. Considering the helical angle $\alpha \geq 70°$, the cross-section shape can be reasonably assumed as elliptical (Jiang, 1999) and its equation is expressed as

$$\left(\frac{x}{R/\sin\alpha}\right)^2+\left(\frac{y}{R}\right)^2=1 \tag{1}$$

For an arbitrary point $P(x_1, y_1)$ on the ellipse, the slope can be determined upon dividing by *dx*

$$\frac{dy}{dx}=\pm\frac{x_1\sin^2\alpha}{R\sqrt{1-\left(\frac{x_1\sin\alpha}{R}\right)^2}} \tag{2}$$

Moreover, the slope at the point $P(x_1, y_1)$ is also equal to $-\tan(\frac{\pi}{2}-\frac{\pi}{m}+\frac{\beta}{2})$. Hence

$$\tan(\frac{\pi}{2}-\frac{\pi}{m}+\frac{\beta}{2})=\frac{x_1\sin^2\alpha}{R\sqrt{1-\left(\frac{x_1\sin\alpha}{R}\right)^2}} \tag{3}$$

Solving equation (3), the solution for x_1 yields

$$x_1=\frac{R}{\sin\alpha}\tan(\frac{\pi}{2}-\frac{\pi}{m}+\frac{\beta}{2})\cdot\frac{1}{\sqrt{\sin^2\alpha+\tan^2(\frac{\pi}{2}-\frac{\pi}{m}+\frac{\beta}{2})}} \tag{4}$$

whereas Eq. (1) results in

$$y_1=\frac{R\sin\alpha}{\sqrt{\sin^2\alpha+\tan^2(\frac{\pi}{2}-\frac{\pi}{m}+\frac{\beta}{2})}} \tag{5}$$

The helix radius for the arbitrary helical wire shown in Fig. 2 can be calculated

$$r = b_1 + y_1 = R\sqrt{1+\frac{\tan^2(\frac{\pi}{2}-\frac{\pi}{m}+\frac{\beta}{2})}{\sin^2\alpha}} \tag{6}$$

(b) establish and solve the one-dimensional problem

As shown in Fig. 1, the equation of elliptical O_3 can be expressed as

$$f_3(x,y)=\frac{\left[x\cos(\pi/m)-y\sin(\pi/m)\right]^2}{(R_3/\cos\alpha_3)^2}+\frac{\left[y\cos(\pi/m)+x\sin(\pi/m)-r_3\right]^2}{R_3^2}=1 \tag{7}$$

Similarly, the equation of elliptical O_2 can be expressed as

$$f_2(x,y)=\frac{x^2}{(R_2/\cos\alpha_2)^2}+\frac{(y-r_2)^2}{R_2^2}=1 \tag{8}$$

The parameters R_3 and α_3 are calculated by using the known strand diameter as the conventional method. Then $f_3(x,y)$ can be determined and $f_2(x,y)$ can be written as the function of R_2 and α_2. Given the geometric characteristic of the Seale strand, that is each layer wires having the same pitch length $p_2 = p_3$, R_2 can be expressed as the function of α_2, i.e.

$$R_2=\frac{r_3\tan\alpha_2}{\tan\alpha_3\sqrt{1+\frac{\tan^2(\frac{\pi}{2}-\frac{\pi}{m}+\frac{\beta}{2})}{\sin^2\alpha_2}}} \tag{9}$$

Now, the one-dimensional function $f(x,y)$, which has only on parameter of α_2 is expressed as

$$f(x,y)=f_3(x,y)-f_2(x,y) \tag{10}$$

Let $f(x,y)=0$, the one-dimensional problem is established. Golden section method is applied to solve the problem. The range of α_2 is from 0 to α_3 on the basis of the geometry characteristic of the Seale strand.

(c) calculate geometric parameters of wires

Through processes 1 and 2, the geometric parameters of the 2nd layer wires and the 3rd layer wires, i.e. R_2, R_3, α_2, α_3, p_2, p_3, r_2 and r_3, can be calculated referring to equations detailedly listed in reference (Pan and Qiu, 2008). The center wire is straight round wires, thus only the radius R_1 is needed.

$$R_1=r_2-R_2 \tag{11}$$

Since Seale strand analyzed is single-lay strand, thus wires geometric model can be built by using spiral parameter equation which can be determined based on above parameters. A three-layered Seale strand geometric model established using the newly developed design method is shown in Fig. 1.

3 FINITE ELEMENT MODEL

The three-layered Seale wire strand analyzed in this paper exhibits excellent helical symmetry and cyclic symmetry. Thus the FEM can be reduced to develop a representative "basic sector" model according to reference (Jiang, 1999). Taking advantage of the strand feature noted above, only a small helical slice of 1/*n* of the strand is needed to model. Fig. 3 shows the slice model, which comprises 1/n of the center wire, one half of a second layer wire and one half of the third layer wire contacting with the selected second layer wire. Fig. 3 also shows the "matching edges", i.e. the lines and their corresponding lines $L_1 - L_2$, $L_3 - L_4$, and area and its corresponding $A_1 - A_2$. θ_s is the sector angle denoting the rotation angle for the matching edges and it can be arbitrarily chosen between $1° - 3°$ (Jiang, 2008). z_s is the sector length and it is calculated using $z_s = p \cdot \theta_s / 2\pi$. The z_s represents the correct strand helical angle, thus its value should not too small to cause numerical problems.

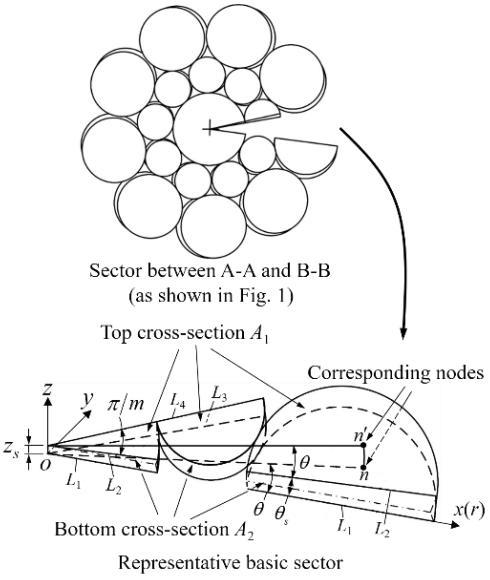

Figure 3. Geometry structure of representative slice model and its matching edges

Fig. 4 shows the finite element mesh of the representative slice geometric model. A much finer mesh was applied in the contact region for the rapid variation of stress. The "matching edges" have corresponding nodes in the FEM. A commercial software ANSYS was used throughout. Three-dimensional solid brick elements were used for

structural discretization. The element is defined by eight nodes each having three degrees of freedom, i.e. translations in *x*, *y* and *z* directions. Surface-to-surface contact elements were used to simulate the contact behavior between wires. This element is able to simulate the general surface-to-surface contact with Coulomb friction sliding.

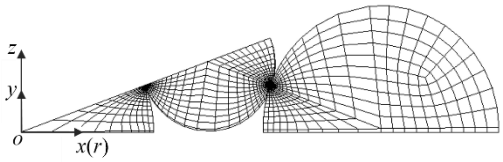

Figure 4. Finite element model of the representative slice model

In order to achieve correct deformation, precise boundary conditions were established by using the constraint equations which relate the displacements of corresponding nodes on the "matching edges". When extension load is applied at the two ends of the Seale strand, the "matching edges" should still remain as "matching edges" after deformation.

The deformation relationships between arbitrary pair of corresponding nodes $n(r,\theta,0)$ and $n'(r,\theta+\theta_s,z_s)$ on the top and bottom cross-sections must satisfy

$$\Delta r' = \Delta r,\ \Delta\theta' = \Delta\theta,\ u_z' = u_z + \delta z_s \tag{12}$$

where Δr, $\Delta\theta$, u_z and $\Delta r'$, $\Delta\theta'$, u_z' are the displacement components of the two nodes n and n' in the cylindrical coordinate system respectively. δz_s is the applied extension between the two cross-sections, $\delta z_s = \varepsilon z_s$, where ε is the strand mean axial stain.

In the Cartesian coordinates, the constraint equations (12) can be transformed as

$$\begin{pmatrix} u_x' \\ u_y' \\ u_z' \end{pmatrix} = \begin{bmatrix} \cos(\theta_s) & -\sin(\theta_s) & 0 \\ \sin(\theta_s) & \cos(\theta_s) & 0 \\ 0 & 0 & 1 \end{bmatrix} \begin{pmatrix} u_x \\ u_y \\ u_z \end{pmatrix} + \begin{pmatrix} 0 \\ 0 \\ \delta z_s \end{pmatrix} \tag{13}$$

where u_x, u_y, u_z and u_x', u_y', u_z' are the displacement components of the node n and its corresponding node n' in the Cartesian coordinate system respectively.

In addition, the four radial corresponding straight lines L_1, L_2, L_3 and L_4 should remain straight, parallel respectively and perpendicular to the symmetric axis *z* after deformation. Hence, the corresponding nodes located on these lines should satisfy both straight line deformation conditions and helical symmetric boundary conditions. The rigid rotation movement of the model is eliminated, which is realized by setting $\Delta\theta = 0$ on these lines. The constraint equations implemented on the corresponding nodes on the four lines can be summarized as follows:

For nodes on line L_1, the displacement components u_y and u_z should meet

$$u_y = 0,\ u_z = 0 \tag{14}$$

For corresponding nodes on L_2, their displacement components of u_x', u_y' and u_z' are related to the u_x of the nodes on L_1 and constraint equations can be written as

$$u_x' = u_x\cos\theta_s,\ u_y' = u_x\sin\theta_s,\ u_z' = \delta z_s \tag{15}$$

Similarly, for nodes on line L_3, the constraint equations are

$$u_y = u_x\tan(\pi/m),\ u_z = 0 \tag{16}$$

For corresponding nodes on L_4, the constraint equations can be written as

$$u_x' = u_x(\cos\theta_s - \sin\theta_s\tan(\pi/m)) \tag{17a}$$

$$u_y' = u_x(\sin\theta_s + \cos\theta_s\tan(\pi/m)) \tag{17b}$$

$$u_z' = \delta z_s \tag{17c}$$

The constraint equations established are all linear and thus they can be conveniently incorporated into the ANSYS system equations. The loading process is realized by gradually applying the stepped sector length increment δz_s.

4 FINITE ELEMENT ANALYSIS RESULTS AND DISCUSSION

The geometry construction of a three-layered 19-wire Seale strand has been designed using the strategy presented in this paper. The helical angle of the third layer wires is $\alpha_3 = 75°$ and wire radius is $R_3 = 2\,\text{mm}$. The included angles between the neighboring helical wires in the second layer wires and the third layer wires are $\beta_2 = \beta_3 = 0.5°$. This ensures that each helical wires in the same layer do not touch each other. The geometry data of the 19-wire Seale strand is summarized in Table 1.

Responses to axial load for the 19-wire Seale strand have been analyzed in this paper. The FEM is shown in Fig. 4, which is only 1/18 of the strand sector between A-A and B-B. The total number of nodes is 3106 and the total number of solid elements is 1425 in the model. The Von Mises yield criterion was assumed. Both a linear elastic material model and an elastic-plastic material model with the bilinear isotropic hardening relation were used. The Young's modulus is 188GPa, Poisson's ratio is 0.3, and yield

stress is 1.54GPa and the plastic modulus in the bilinear elastic-plastic case is 24.6GPa. Zero friction was assumed between all contact surfaces on the basis of good lubrication.

Table 1. The geometry data of the three-layered 19-wire Seale strand

Strand diameter	16.21mm
Pitch length p	143.13mm
Center wire diameter $2R_1$	4.5mm
The 2nd wire diameter $2R_2$	2.26mm
The 3rd wire diameter $2R_3$	4.0mm
Helical angle of the 2nd layer wire α_2	81.56°
Helical angle of the 3rd layer wire α_3	75°

In this analysis, a strand axial strain $\varepsilon = 0.01$ was applied in increments of 0.00025. The numerical results have been compared with those from Costello's elasticity analytical model where applicable (Costello, 1997). Fig. 5 shows axial load as a function of strand axial strain. Fig. 6 gives the variation of strand axial torque with the applied axial strain. It can be seen from these two figures that the finite element analysis results in the linear elasticity region ($\varepsilon \le 0.008$) are very close to the results predicted by using Costello's elastic theory.

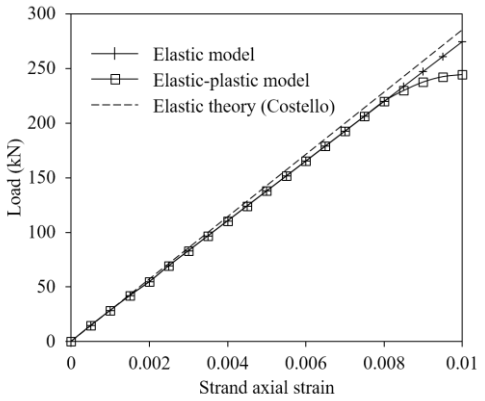

Figure 5. Variation in axial load with strand axial strain

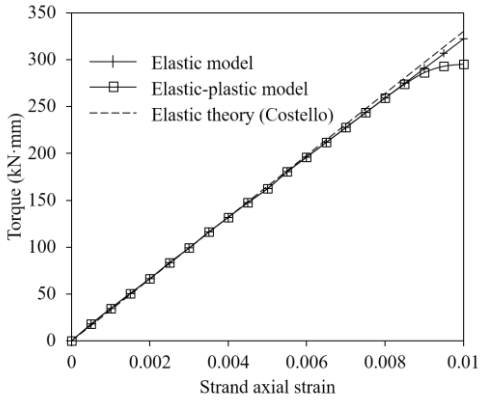

Figure 6. Variation in torque with strand axial strain

Sample colour contour plots of stress are also presented at a strand axial strain of 0.004, which is a typical loading level for engineering applications. Fig. 7(a) shows the global axial stress distribution, σ_z, and Fig. 7(b) shows the von Mises equivalent stress, σ_{eqv}. It can be seen from these two figures that the value of the axial stress in the bulk of wires (ignoring the contact regions) is approximately equal to that of the Von Mises equivalent stress. This indicates that axial stress σ_z is the predominant stress. Moreover, it can be seen from Fig. 7(b) that the stress peak caused by the contact between center wire and the second layer wires, $\sigma_{1\max} = 1547\,\text{MPa}$, is slightly higher than that caused by the contact between the second layer wires and the third layer wires, $\sigma_{2\max} = 1312\,\text{MPa}$, and the relative deviation is only 15%.

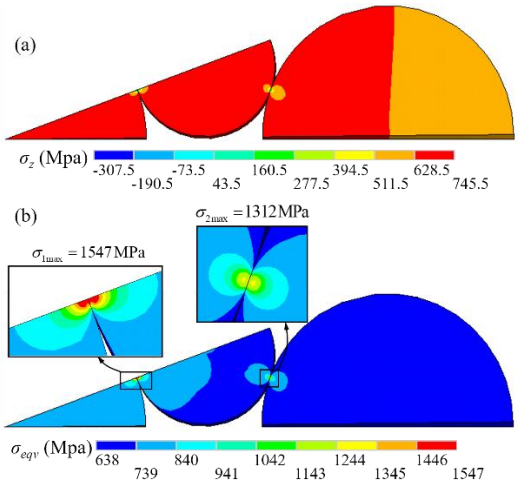

Figure 7. Stress distribution at a strand axial strain of 0.004 (a) axial stress σ_z and (b) Von Mises equivalent stress σ_{eqv}

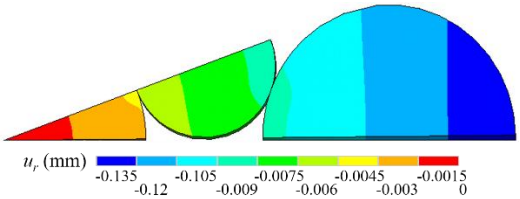

Figure 8. Contour plot of radial displacement, u_r, at a strand axial strain of 0.004

Sample colour contour plot of radial displacement u_r at a strand axial strain of 0.004 is presented in Fig. 8. As expected, there exists obvious radial contraction when strand is subjected to axial tensile load.

Fig. 9 shows the variation of changes in helix radius of the helical wire centerlines with strand axial strain. It can be seen from this figure that there exists a marked departure when the bulk of strand material

begins to yield, i.e. for strand axial strains reaching approximately 0.008 as shown in Fig. 5.

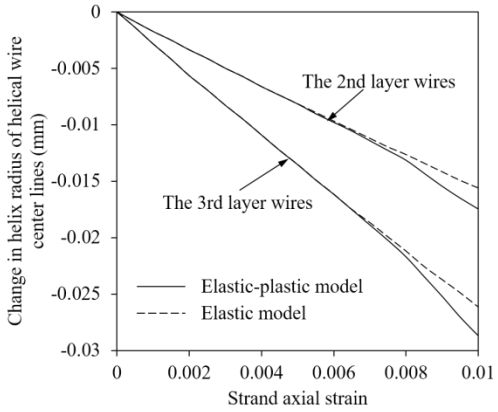

Figure 9. Variation of changes in helix radius of helical wire centerlines with strand axial strain

Fig. 10 gives the colour contour plot of circumferential displacement at a strand axial strain of 0.004. Fig. 11 shows the variation of the circumferential displacement of helical wire centerlines with strand axial strain. It can be seen from Fig. 11 that in the linear elasticity region, the variation of circumferential displacement with strand axial strain is nearly linearity. When strand axial strain increases beyond 0.008, the results predicted from elastic-plastic model are obvious higher than those analysed by using the elastic model. Furthermore, it can be seen from these two figures that the circumferential deformation is small compared to axial and radial displacement. For the 19-wire Seale strand analysed in this paper, when the axial load is in the linear elasticity region, the maximum value of circumferential displacement, i.e. the rotation angle in the cylindrical coordination system, is nearly 0.0042. This indicates that if the predefined included angle $\beta > 0.0042$, it can ensure that adjacent helical wires in the same layer will not touch each other.

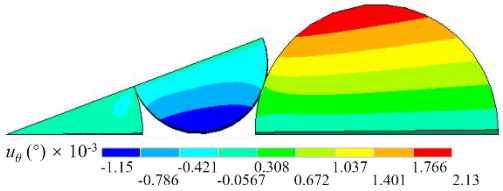

Figure 10. Contour plot of circumferential displacement, u_θ, at a strain axial strain of 0.004

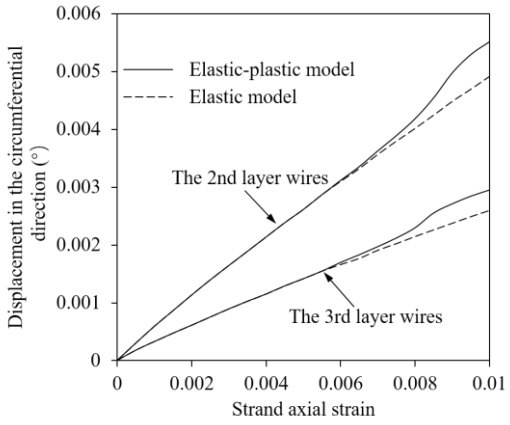

Figure 11. Variation of circumferential of helical wire centerlines with strand axial strain

Fig. 12 shows maximum contact pressures against strand axial strain. Elastic-plastic finite element analysis shows that the local contact area between center wire and the second layer wires begins to yield first when the applied axial strain is nearly 0.004, whereas the material in the local contact between the second layer wires and the third layer wires begins to yield when the axial strain reaches approximately 0.00525. Moreover, it can be seen from this figure that when local wire material enters into plasticity, the increment of the maximum contact pressures decreases with the increasing strand axial strain for both of the two contact locations.

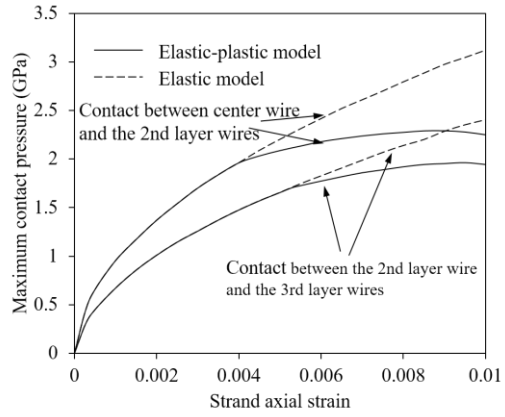

Figure 12. Variation of maximum contact pressures with strand axial strain

To illustrate the influences of helical angle, the predefined helical angle of the third layer wires α_3 varying from 70° to 85° by increment of 5° has been analysed. Table 2 presents the analysis results of average normalised maximum contact pressures, which is defined as $\sigma_{c\max}/(E\sqrt{\varepsilon})$, in the elastic region. The range of strand axial strain applied to the

elastic analyses is $\varepsilon = 0 - 0.006$. As the helical angle of α_3 is increased, the normalised maximum contact pressures for both contact locations decrease obviously, whereas the ratio between the two normalised maximum contact pressures only has slight increase.

Table 2. Normalized maximum contact pressures

Helical angle of the 3rd layer wires α_3 (°)	Wire radius ratio $R_1 : R_2 : R_3$	Normalized maximum contact pressure $\sigma_{c\max}/(E\sqrt{\varepsilon})$	
		Between center wire and the 2nd layer wires	Between the 2nd layer wires and the 3rd layer wires
70	1.1726:0.5824:1	0.2089	0.1641
75	1.1250:0.5659:1	0.1657	0.1254
80	1.0929:0.5543:1	0.1137	0.0836
85	1.0742:0.5474:1	0.0556	0.0403

5 CONCLUSION

A new geometry design method of three-layered 19-wire Seale strand, which can arbitrarily predefine the included angel between adjacent helical wires in the same layer, has been presented in this paper. The problem of deriving the diameter ratio of each layer wires has been established into a one-dimensional problem and efficient golden section method has been applied to solve the problem. Compared with gradual approaching method used in the conventional method, the newly proposed method can greatly improve calculation precise and computational efficiency. A concise FEM, which takes into account of the helical symmetry and cyclic symmetry of the three-layered Seale wire strand geometric structure, has also been developed to predict the strand axial tensile behavior. Numerical results show that for the three-layered 19-wire Seale strand loaded in the linear region, the contacts between neighboring helical wires can be avoided when included angle is predefined beyond 0.0042°. Furthermore, contact behavior between adjacent wire layers and effects of wire helical angles have also been predicted effectively by using the newly developed FEM. The methodology proposed in this paper can be extended to geometrical design and mechanical behavior analysis for the Seale wire strand with more complex cross-section.

6 ACKNOWLEDGMENT

This work is supported by A Project of Shandong Province Higher Educational Science and Technology Program (KJ2018BBB043) and Doctoral Scientific Research Foundation of Zaozhuang University (2017BS05)

7 REFERENCES

Chen, Y. P., F. M. Meng and X. S. Gong, (2015). Parametric modeling and comparative finite element analysis of spiral triangular strand and simple straight strand, *Advances in Engineering Software*. 90, 63-75.

Costello, G. A. (1997). Theory of wire rope, 2nd ed. *Springer, New York*.

Cruzado, A. M. and A. Urchegui, (2014). Finite element modeling of fretting wear scars in the thin steel wires: Application in crossed cylinder arrangements, *Wear*, 318, 98-105.

Erdönmez, C. & C. E. Imrak, (2011). Modeling techniques of nested helical structure based geometry for numerical analysis, *Journal of Mechanical Engineering*. 57(4), 283-292.

Fontanari, V., M. Benedetti and B. D. Monelli, (2015). Elasto-plastic behavior of a Warrington-Seale rope: Experimental analysis and finite element modeling, *Engineering Structures*. 82, 113-120.

Ghoreishi, S. R., T. Messager, et al, (2007). Validity and limitations of linear analytical models for steel wire strands under axial loading, using a 3D FE model, *International Journal of Mechanical Sciences*, 49(11), 1251-1261.

Jiang, W. G., M. S. Yao and J. M. Walton, (1999). A concise finite element model for simple straight wire rope strand, *International Journal of Mechanical Sciences*. 41, 143-161.

Jiang, W. G., M. K. Warby and J. L. Henshall, (2008). Statically indeterminate contacts in axially loaded wire strand, *European Journal of Mechanics A/Solids*. 27, 69-78.

Jiang, W. G. & J. L. Henshall, (1999). The analysis of termination effects in wire strand using the finite element method, *Journal of Strain Analysis for Engineering Design*. 34(1), 31-38.

Jiang, W. G., J. L. Henshall and J. M. Walton, (2000). A concise finite element model for three-layered straight wire rope strand, *International Journal of Mechanical Sciences*. 42, 63-86.

Judge, R., Z. Yang and S. W. Jones, et al (2012). Full 3D Finite element modelling of spiral strand cables, *Construction and building Materials*. 35, 452-459.

Judge, R., Z. Yang and S. W. Jones, et al (2017). Spiral strand cables subjected to high velocity fragment impact, *International Journal of Impact Engineering*. 107, 58-79.

Nawrocki, A. & M. Labrosse, (2000). A finite element model for simple straight wire rope strands, *Computers and Structures*, 77, 345-359.

Pan, Z. Y. & M. H. Qiu, (2008). Production technology of wire rope. *Hunan University Press, Hunan*.

Páczelt, I. & R. Beleznai, (2011). Nonlinear contact-theory for analysis of wire rope strand using high-order approximation in the FEM, *Computers and Structures*. 89, 1004-1025.

Stanova, E., G. Fedorko and M. Fabian, (2011). Computer modelling of wire strands and ropes Part II: Finite element-based applications, *Advances in Engineering Software*. 42, 322-331.

Stanova, E., G. Fedorko and M. Fabian, (2011). Computer modelling of wire strands and ropes Part I: Theory and computer implementation, *Advances in Engineering Software*. 42, 305-315.

Stanova, E., G. Fedorko and S. Kmet, et al (2015). Finite element analysis of spiral strands with different shapes subject to axial loads, *Advances in Engineering Software*. 83, 45-58.

Sun, T. G. & T. L. Shi, (2016). Mathematical model and finite element analysis of wire ropes, *Journal of Wuyi University (Natural Science Edition)*. 20(1), 64-68.

Wang, X. Y., X. B. Meng and J. X. Wang, et al (2015). Mathematical modeling and geometric analysis for wire rope strands, *Applied Mathematical Modelling*. 39, 1019-1032.

Yu, Y. J., X. X. Wang and Z. H. Chen, (2016). A simplified finite element model for structural cable bending mechanism, *International Journal of Mechanical Sciences*. 113, 196-210.

Yu, C. L., W. G. Jiang and L. J. Yan, (2016). Analysis and modeling of socket termination for wire strand using finite element methods, International Journal of Simulation Systems, Science & Technology, 17(29), 241-246.

Yu, C. L., W. G. Jiang and C. Liu, (2017). A beam finite element model for efficient analysis of wire strands, *International Journal of Performability Engineering*. 13(3), 315-322.

Zhao, P., H. Wang and X. S. Tian, et al. (2017). Construction of mathematical model for the bending state of braided wire rope, *Advances in Computer Science Research*. 71, 1421-1425.

Zhou, W. & H. Q. Tian, (2013). A novel finite element model for single-layered wire strand, *Journal of Central South University*. 20, 1767-1771.

Jie Sheng, Peiqing La, Jiaqiang Sux, Junqiang Renz; yy, Ji qiang Maz, Yu Shi, Zhengning Li and Jiao Wang, (2018).In situ SEM analysis for deformation mechanism of micro/nanostructured 304 stainless steel with high strength and good plasticity. 32, 12

D. Zhou, K. Zhang, A. Ravey, F. Gao, A. Miraoui, (2016).Parameter Sensitivity Analysis for Fractional-Order Modeling of Lithium-Ion Batteries, *Energies*, 9, 123.

D. Zhou, K. Zhang, A. Ravey, F. Gao, A. Miraoui, (2016). On-Line Estimation of Lithium Polymer Batteries State-of-Charge Using Particle Filter Based Data Fusion with Multi-Models Approach, *IEEE Transactions on Industry Applications*, 52, 2582-2595.

8 NOTES ON CONTRIBUTORS

Dr. Chunlei Yu is a researcher at Zaozhuang University, China. His major research interests include mechanical simulation of wire rope and construction machinery. He has published many papers about his research area.
Email: yclfinder@163.com

Mr. Binjie Dong is a mid-level engineer at Shijiazhuang King Transportation Equipment CO., LTD, China. His major research interests include design and simulation of machinery and equipment.
Email: bin-jie.dong@foxmail.com